Mat. Res. Soc. Symp. Proc. Vol. 674 © 2001 Materials Research Society

In-Situ Characterization Of Ultra-Small Magnetic Junctions Made By Electrochemical Techniques

A. Sokolov, J.R. Jennings, C-S Yang, J. Redepenning[1] and B. Doudin
Department of Physics and Astronomy, [1] Department of Chemistry
University of Nebraska-Lincoln, Lincoln NE 68588-0111, U.S.A.

ABSTRACT

Electrochemical impedance spectroscopy is used to characterize the growth of NiO over Ni electrodes. We find a limited increase of thickness and a significant increase of porosity of the oxide as a function of time and anodization potential. Conductance measurements performed on Ni/NiO/Co junctions of 30 nm diameters indicate the presence of a Coulomb blockade at low temperatures and small bias. Tunneling is observed at higher bias. Small magnetoresistance ratios (1%) are found.

INTRODUCTION

Synthesis of a metal/insulator/metal system by electrochemical techniques is presented. We use template methods to make ultra-small ferromagnetic tunnel junctions, of interest for studying magnetoresistive sensors. The conductance of a ferromagnet/insulator/ferromagnet system is modified when switching the magnetic alignment of the two ferromagnetic contacts between parallel and antiparallel configurations [1, 2]. This junction magnetoresistance is of interest for making new types of magnetic sensors and memories [3]. The electrochemical technique we use is an original method for making such structures, and junctions with areas as small as 0.008 μm^2 can be prepared and investigated. Our first results showed remarkably large magnetoresistance (MR) effects in such junctions, and a model of conductance governed by impurity states in the barrier has been put forward [4]. Theoretical models of interplay between Coulomb blockades and tunnel magnetoresistance have been published recently [5 - 7]. In light of these models, our goal is to investigate the extent to which the MR in our systems is due to thermally enhanced sequential tunneling, co-tunneling [5] or spin accumulation [6, 7].

In-situ investigations during the synthesis of the insulating barrier are helpful in understanding and in controlling the morphological and electrical properties of the oxide barrier. We modulate the electrochemical process necessary to grow the barrier with an AC excitation. By monitoring the frequency dependent response of the system to this excitation, we can thus monitor and quantify the growth of the insulating oxide in-situ. Electrochemical impedance spectroscopy (EIS) is a well-established characterization method, and we can take advantage of the abundant literature on corrosion studies to compare our results with those obtained for other dielectric layers on conductors in electrochemical baths [8]. Under appropriate experimental conditions we are able to decouple the impedance of the electrochemical bath from the impedance due to the oxide coating. Correlation between the electric conductance of the metal-insulator-metal system and the EIS of the metal/insulator electrode gives a clearer picture of the morphology of the insulating oxide.

EXPERIMENTAL

Polycarbonate track-etched membranes were used as templates for the electrodeposition of wires with lengths of 7 μm and diameters as small as 30 nm [9]. Ni half-wires were plated using a Watt's bath. Anodization of Ni was performed in 0.075 M sodium borate and 0.3 M boric acid solution [10]. The Co overlayer was plated using a non-aqueous bath comprised of 0.1M cobalt chloride (anhydrous) in dimethylformamide or ethylene glycol. Deposition of the cobalt overlayer was performed in a nitrogen atmosphere (containing less than 3 ppm of oxygen and water) to eliminate side reactions possible during the Co plating [4].

EIS studies were performed in the sodium borate bath during the anodization process. A frequency response analyzer coupled with an electrochemical interface was used to record the spectrum. Figure 1 shows a theoretical EIS spectrum of a thin dielectric coating of a metal, with the corresponding equivalent circuit. Extensive literature can be found on the subject [11]. At high frequencies the kinetics of the redox processes (elements R1, C1 and R2a) dominate the response. This is manifested by a high-frequency half-circle in the Nyquist plot (Figure 1). In mid range frequencies, the dielectric thin film contributes through elements R2b, R3 and CPE1 to the second half-circle of the spectrum. The constant phase element expresses a frequency-dependent capacitance that is observed for very thin films. In detailed analysis, deviations from perfect capacitance can be interpreted in terms of film porosity. At low frequency, the dominant mass transfer process is represented by the lumped elements W1 (Warburg impedance), R4 and CPE2. Ex-situ electrical connections were made to single wires by monitoring the deposition current as described previously[12]. Low temperature investigations were performed in a helium cryostat under magnetic field of ± 10 T range.

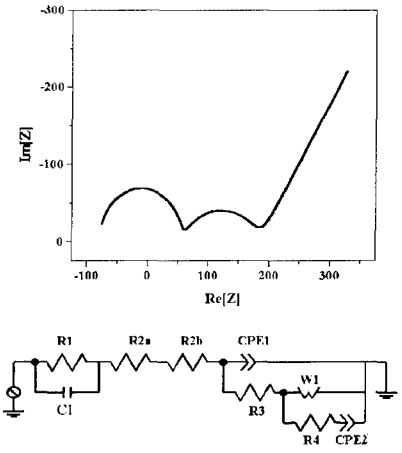

Figure 1. Nyquist plot of a theoretical electrochemical impedance spectrum, with the related equivalent circuit. The dielectric coating is represented by the lumped elements R2b, CPE1 and R3.

RESULTS

Systematic measurements of the EIS spectrum of Ni/NiO systems were performed as a function of time and anodization potential. Figure 2 shows the evolution of the spectrum with time. The half circle at mid-range frequencies (between and 1 kHz and 100 kHz typically) can be attributed to the presence of a dielectric layer on the electrode surface; however, care should be exercised in making a quantitative interpretation of the data. In-situ EIS is advantageous because the insulator of interest can be characterized as it is grown. Unfortunately, the impedance of the bath is convolved with that of the circuit elements of interest. For example, the low impedance values found at low frequencies are associated with mass transfer processes. As a result, reliability of absolute values for the insulator properties is decreased when chemical processes occur. Qualitative information can be obtained by measuring the time evolution of the EIS response at a frequency (e.g., 5 kHz) where changes in the dielectric properties of the barrier are particularly evident. After a rapid initial growth phase that occurs over a few tens of seconds, the capacitance associated with the oxide barrier increases slowly with anodization time. Figure 3 demonstrates the influence of the anodization potential on the capacitance. The imaginary part of the impedance *decreases* as the potential of the anode is made more positive. It also *decreases* with increased anodization time. The related increase in capacitance indicates an increase in the effective area of the oxide and a limit to the maximum thickness that can be achieved. In other words, we find that the porosity of the nickel oxide increases with time and anodization potential. This result confirms previous studies of anodized nickel that suggest the presence of a thin NiO film of a few atomic layers which becomes more porous upon extended anodization [13]. After plating the top Co half-wire, we investigated the current-potential response of a series of samples at low temperatures (Figure 4). We observed a systematic decrease of the sample conductance when increasing the anodization potential. At low bias a majority of the sample showed a low conductance that can be attributed to blocking of electron flow by an electrostatic energy $E_c = e^2/2C$, where C is the capacitance between the blocking island and current source and drain. At the limit of zero temperature, no current flows for voltage bias smaller than e/2C.

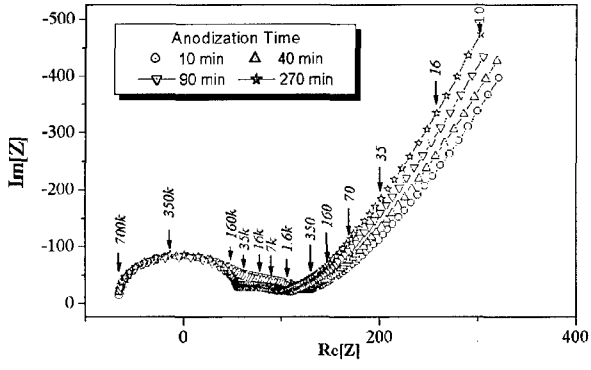

Figure 2. The observed impedance spectrum of anodized Ni for several anodization times.

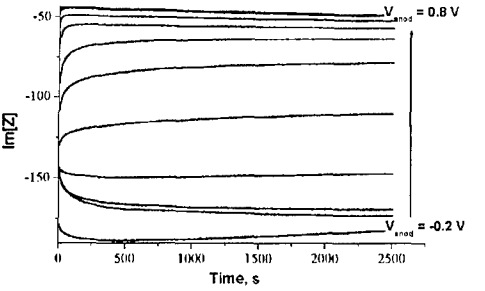

Figure 3. Time evolution of the imaginary part of the impedance at 5 kHz, for several anodization potential values. In a first approximation –Im(Z) can be interpreted as the inverse of the oxide film capacitance.

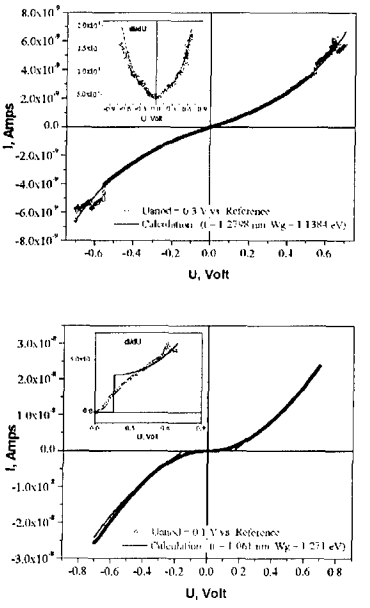

Figure 4. IV curves of Ni/NiO/Co nanowires of 30 nm diameters. Inserts are derivatives of the curves, with the corresponding fittings using tunneling (left) of Coulomb blockade at low bias and tunneling at high bias (right).

One can express the current due to tunneling through a barrier of width t and height W_g, by the equation

$$J = \frac{e}{2\pi\hbar}\frac{1}{t^2}\left\{\left(Wg - \frac{eV}{2}\right)Exp\left[-Ct\left(Wg - \frac{eV}{2}\right)^{1/2}\right] - \left(Wg + \frac{eV}{2}\right)Exp\left[-Ct\left(Wg + \frac{eV}{2}\right)^{1/2}\right]\right\}$$

which corresponds to a quadratic conductance versus voltage in first approximation [14]. Values of t and W_g are fit to the above equation in the set of four samples shown in Figure 4. A value of 0.008 μm^2 is used for the area of all the junctions. This is a rough estimate corresponding to the geometric cross-section area of the nanowires. The porosity of the oxide increases this value, but filamentary conduction will occur through a limited fraction of the junction, reducing its effective area. The barrier thickness and height contribute exponentially to the conductance, and fitted values of typically 1 eV for the barrier height and 1 nm for its thickness account for the whole set of investigated samples.

No significant change of conductance with temperature is expected for a tunneling barrier of energy height much larger than kT. The significant conductance variation we observe at temperatures higher than a few tens of K (Figure 5) is inconsistent with the simple model presented above. The electronic conductance of our junctions increases when the temperature is increased, apparently because intermediate energy levels become thermally accessible. Consequently, at "high" temperatures, a semiconductor-type conduction plays the dominant role. The classical expression is of the form:

$$J = V(N_0 N_d)^{1/2} Exp\left(-\frac{W_d - eV}{2k_B T}\right), \text{ where } N_0 \equiv 2\left(m_e k_B T / h^2\right)^{3/2}$$

where N_d is the donor concentration and W_d is the donor activation energy. To summarize, our samples show three conduction regimes: a Coulomb blockade regime at low voltage bias and low temperatures, a tunneling regime at high voltage bias and low temperatures, and a regime at high temperatures where conduction is mediated by defects in the barrier.

Magnetoresistance measurements are shown in Figure 6. We found small MR amplitudes, rapidly decreasing with voltage bias. These values are reminiscent of results found on NiO junctions made by vacuum techniques [15], and do not reach the large values previously found on larger nanowires (diameter 80 – 100 nm). A possible explanation is the lower conductance of this new series of samples, making the process of co-tunneling very unlikely [5]. The enhancement of the MR is therefore of low probability and we find that a sequential tunneling thermally enhanced through a Coulomb blockade does not show large MR effects.

The supports from NSF CAREER DMR 98-74657, NSF REU SITE program DMR 97-32056 (J.R. J.) and the Nebraska Research Initiative are gratefully acknowledged.

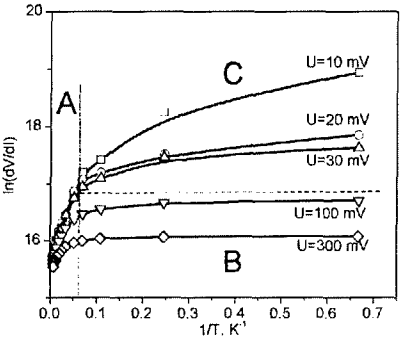

Figure 5. Temperature evolution of the conductance, measured at several different voltage bias. The conduction regimes are indicated by A: Coulomb blockade, B: tunneling, C: semiconducting.

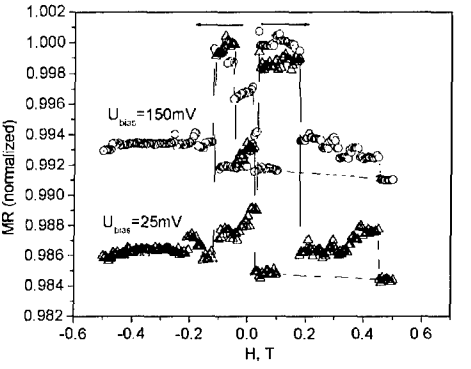

Figure 6. Magnetoresistance curves at 5 K, for two different voltage bias. The resistance is normalized to the antiparallel state value.

REFERENCES

1. M. Julliere, *Phys. Lett.* **54A**, 225 (1975).

2. J. S. Moodera, L. R. Kinder, T. M. Wong and R. Meservey, *Phys. Rev. Lett.* **74**, 3273 (1996)

3. W. J. Gallagher, S. S. P. Parkin, Yu Lu, X. P. Bian, A. Marley, K. P. Roche, R. A. Altman, S. A. Rishton, C. Jahnes, T. M. Shaw and Gang Xiao, *J. Appl. Phys.* **81**, 3741 (1997).

4. B. Doudin, S. Gilbert, G. Redmond, J.-Ph. Ansermet, *Phys. Rev. Lett.* **79**, 933 (1997).

5. S. Takahashi and S. Maekawa, *Phys. Rev. Lett.* **80**, 1758 (1998).

6. J. Barnas and A. Fert, *Phys. Rev. Lett.* **80**, 1058 (1998)

7. A. Brataas, Y. V. Nazarov, J. Inoue and G. E. Bauer, *Phys. Rev. B* **59**, 93 (1999).

8. J. R. Macdonald, *Impedance spectroscopy: emphasizing solid materials and systems*, John Wiley & Sons, New York, (1987).

9. C. R. Martin, *Science* **266**, 1961 (1994)

10. B. MacDougall and M. J. Graham, *J. Electrochem. Soc.* **128**, 2321 (1981).

11. M. Duprat, Ed. *Electrochemical Methods in Corrosion Research*, Materials Science Forum, Vol 8 (1986).

12. J.E. Wegrowe, S.E. Gilbert, D. Kelly, B. Doudin, J.-Ph. Ansermet *IEEE Trans. on Mag.* **34**, 903 (1998).

13. G. Dagan, W.-M. Shen and M. Tomkiewicz, *J. Electrochem. Soc.* **139**, 1855 (1992).

14. J. G. Simmons, *J. Appl. Phys.* **34**, 1793 (1963)

15. T. Miyazaki and N. Tezuka, *J. Mag. Mag. Mater.* **151**, 403 (1995).